THE JOURNAL OF PHYSICAL CHEMISTRY A

 VOLUME 104, NUMBER 43, NOVEMBER 2, 2000

FEATURE ARTICLE

Charge Flow and Solvent Dynamics in the Photodissociation of Solvated Molecular Ions

R. Parson,* J. Faeder,† and N. Delaney

JILA, University of Colorado and National Institute of Standards and Technology, and Department of Chemistry and Biochemistry, University of Colorado, Boulder, Colorado 80309-0440

Received: May 31, 2000

We survey recent experimental and theoretical studies of photodissociation and recombination of dihalide ions in gas-phase clusters and liquid solution. A crucial property of these systems is the flow of excess charge within the solute, which is strongly coupled to the motion of the surrounding molecules. Using a model inspired by the theory of electron-transfer reactions, we have constructed a comprehensive physical picture of the interplay of charge flow and solvent dynamics on multiple, coupled electronic states. The consequences are sometimes surprising: for example, in excited states having antibonding character, the charge moves to the *less* solvated atom as the solute dissociates, leading to more efficient recombination than in neutral systems. Our analysis also predicts extremely efficient spin−orbit quenching (associated with solvent-induced curve crossings) following UV excitation of I_2^- clustered with CO_2, which has been confirmed by experiment and suggests a revised interpretation of the transient absorption peak seen in pump−probe experiments.

I. Introduction

Since chemical bonds are made out of electrons, any chemical reaction involves some redistribution of electronic charge. When a reaction takes place in a cluster, a liquid solution, or a solid matrix, the interaction between the shifting charge and the surrounding molecules can profoundly influence the course of the reaction.[1] The solvent does not then merely interrupt and redirect motion on the potential energy curves of the solute; instead, the reaction must be regarded as taking place on a multidimensional potential energy surface that depends on both solute and solvent coordinates. If electronically excited states are involved, as in photochemical reactions, one must consider several such surfaces, together with the nonadiabatic transitions that couple them.

Experimental studies of the photodissociation and recombination of dihalide anions in gas-phase clusters[2−15] and in liquid solution[16−19] have brought these issues into focus. This work was in large measure inspired by a long series of classic experiments on the "cage effect" in neutral I_2.[20−26] Compared to the neutrals, the ions offer some significant experimental advantages, particularly in the cluster phase since clusters of a desired size can be isolated using a mass spectrometer. However, the ionic systems are more complicated to understand than their neutral analogues since the excess charge interacts strongly with the surrounding solvent. Consider the photodissociation of I_2^-, whose gas-phase potential curves are illustrated in Figure 1. As this molecule dissociates, the electronic charge, which was initially delocalized over the molecule, becomes localized on a single I atom. In a cluster or solution, this flow of charge within the solute will be strongly coupled to the motions of the surrounding molecules, since a compact, atomic charge distribution is more easily solvated than a diffuse, molecular one. The changing solvent environment, in turn, influences the charge localization process. The results of this interplay are sometimes surprising—for example, during the first phase of photodisso-

† Current address: Department of Chemical Physics, Weizmann Institute of Science, 76100 Rehovot Israel.

10.1021/jp0019916 CCC: $19.00
Published on Web 09/30/2000

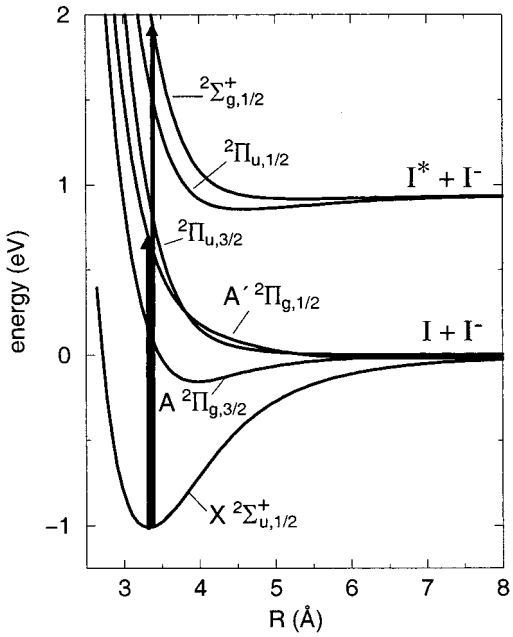

Figure 1. Photodissociation of I_2^- on the gas phase potential curves. The shorter arrow illustrates the IR excitation used in most of the photodissociation studies, while the longer arrow indicates the recently studied UV excitation.

ciation the charge moves toward the *less* solvated atom, a phenomenon that we have called "anomalous charge flow"—and their experimental consequences have been demonstrated.

The purpose of this article is to explain, in simple physical terms, the role of solvent-induced charge flow in the photodissociation of solvated dihalide ions. In the remainder of this introduction we briefly summarize the experimental and theoretical techniques that have been applied to these systems. Section II describes charge flow using a simple molecular orbital picture and presents a few examples of its experimental consequences. Section III presents a deeper perspective on the problem, based on the theory of electron-transfer reactions, and section IV shows how the results of both experiments and simulations can be understood from this point of view. Finally, section V places our work in a larger context and suggests some directions for future research.

Experiments on Dihalide Photodissociation. The experimental story begins with pioneering studies of photodissociation of Br_2^- and I_2^- embedded in size-selected CO_2 clusters, carried out by Lineberger and co-workers.[2,4] In these experiments, a near-infrared (700−800 nm) laser pulse promotes the dihalide ion to the repulsive A′ state (Figure 1), and the branching ratio for dissociation versus recombination is determined from the mass spectra of the ionic photofragments. The fraction of recombined, or "caged", photoproducts was found to rise very rapidly as a function of cluster size, reaching unity by the completion of the first solvation shell. This trend, which was subsequently replicated for I_2^- clustered with Ar,[27] N_2O,[28] and OCS,[8] was surprising given that between 30 and 90% of I_2 dissociates in solution.[23] The rapid onset of caging was attributed to the presence of long-range electrostatic interactions, but the actual mechanism long remained mysterious. More recently, Lineberger and co-workers have carried out analogous experiments using ultraviolet excitation,[8,10] for which the initially excited B state in the isolated molecule correlates to an I^- ion and an I atom in its spin−orbit excited state, I*. They found that a relatively small number of solvent molecules, less than a full solvation shell, was able to cage this highly excited state and induce electronic relaxation all the way down to the ground state.

Lineberger and co-workers also studied these systems in the time domain,[3,5−7,9,28−30] using a laser pulse to dissociate the I_2^- chromophore within the cluster, and a subsequent pulse to probe for return of the absorption as the atoms recombine. Analogous experiments were performed by Barbara and co-workers[16−19] in a variety of liquid solutions. In most cases the time scale for absorption recovery was measured to be about 10−20 ps. Superimposed on the overall recovery curve was a peak occurring at about 2 ps after excitation,[6,29] which was originally attributed to transient recombination on the intermediate A state, although subsequent theoretical work, discussed in section 4, suggests a different mechanism. From these results it was inferred that the overall process of photodissociation, recombination, and vibrational relaxation takes place on a time scale of tens of picoseconds, an order of magnitude faster than for neutral I_2 in solution.[23] In another series of solution phase experiments, Banin, Ruhman, and co-workers observed coherent vibration of the I_2^- product formed by photodissociation of I_3^-.[31−36] While the primary focus of their work was the dynamics of the triodide parent, their results provide additional evidence for fast vibrational relaxation in solvated I_2^-.

A different time-dependent technique, femtosecond photoelectron spectroscopy (FPES) was introduced into this field by Neumark and co-workers.[11,13−15,37] As in the Lineberger experiment, the first pulse in the FPES experiment dissociates the I_2^-, but now the probe pulse, which is in the ultraviolet, detaches the excess electron from the anion. The dependence of the electron kinetic energy spectrum on the time delay between the pump and the probe yields insights into the reaction dynamics that complement those obtained from the absorption recovery experiments. FPES experiments on $I_2^-Ar_6$ have characterized the dynamics of direct dissociation, while the spectra of larger argon clusters directly track the dynamics of electronic and vibrational relaxation.[11,14] The more recent FPES studies on $I_2^-(CO_2)_n$[13,15] demonstrate the importance of charge flow in the dissociation, and confirm the 10−20 ps time scales for recombination in the larger clusters.

Simulations of Dihalide Anion Photodissociation. The first simulations of dihalide anion photodissociation were performed by Perera and Amar,[38,39] who examined Br_2^- dissociation in argon and CO_2 clusters using empirical potentials for the solute, the solvent, and the interaction between them. Only two solute electronic states were included, and nonadiabatic transitions from the excited to the ground state were treated in an ad hoc fashion, by switching the trajectories from one to the other at large internuclear distances. Perera and Amar modeled solute charge flow by assigning a partial charge to each bromine atom that varied as a function of the bond length, so that as the molecule dissociated the charge on one atom decayed to zero while the charge on the other increased to −1. The atom that received the charge was chosen randomly; as a result, in about half of the simulation trajectories the charge ended up on the more favorably solvated atom while in the other half it moved in the opposite direction. Perera and Amar noted that the dissociation dynamics differed markedly in these two cases, and that good agreement with the experimental branching ratios was only achieved when both types of trajectories were retained in the ensemble. Since the charge switching depended only on the solute bond length, the solvent had no direct effect on the solute electronic structure—it could not polarize the dissociating anion. Despite the limitations of their model, Perera and Amar laid

out clearly the fundamental theoretical issues in this area, and to a large extent our own efforts have been devoted to answering the questions that they raised.

For the next few years, theoretical work in this area concentrated on adiabatic dynamics in the electronic ground state. Our group[29,40−42] extended the work of Amar and Perera by allowing the solute charge distribution to depend on the local state of the solvent. Motivated by the theory of electron-transfer reactions in solution,[43−45] we used calculations of the electronic structure of I_2^- in a uniform electric field to parametrize a "charge switching surface" that depended upon two coordinates, the solute bond length and a collective solvent coordinate that represents the net electric field that the solvent exerts on the solute charge distribution. Hynes, Benjamin, Barbara, and co-workers[46−49] approached this problem in a different way, by adapting recent work by the Hynes group in the theory of electronic structure in solution.[50−52] In their approach the I_2^- ground-state potential was fit to a semiempirical Valence Bond Hamiltonian, and the parameters in this Hamiltonian were then taken to be functions of a collective solvent coordinate. Since the electronic wave function of the solute is determined by the valence bond parameters, solvent motion gives rise to solute charge flow in a natural fashion. While these two theoretical treatments are constructed differently, they are similar in spirit: the effects of solvation on solute electronic structure are described by a single collective coordinate representing the asymmetry of the local environment around the solute, and the interaction between solute charge flow (in the electronic ground state) and solvent dynamics is treated self-consistently. Simulations, based on these models, of I_2^- vibrational relaxation in clusters[41] and liquid solution[49] found that this relaxation is very fast, in agreement with the experiments.[16−19] Exceptionally fast relaxation was seen in the upper part of the solute potential well, where the I and I^- are first beginning to recombine—in both simulations, more than half of the total vibrational energy was lost in less than one picosecond. Hynes and co-workers showed that this "ultrafast" initial relaxation is a direct consequence of the interaction between the changing charge distribution and the solvent polarization, which gives rise to a long-range collective force that efficiently removes energy from the solute.[47]

To this point, theory had provided valuable insights into various aspects of the dynamics but had not yet really succeeded in simulating it in full. Amar and Perera had treated both the solute charge distribution and the nonadiabatic transitions in an ad hoc fashion, while the subsequent work had focused on ground-state dynamics. This situation changed in 1996, when Coker and co-workers[53,54] and our own group[55−59] independently developed simulation models that treat solvation effects in ground and excited states in a self-consistent fashion. These models are based on an Effective Hamiltonian approach to the electronic structure of the solvated species, in which a Hamiltonian matrix whose elements are functions of the solvent degrees of freedom is constructed and diagonalized at each time step of a molecular dynamics trajectory. For a given configuration of solvent molecules, the eigenvalues of this matrix specify single points on the multidimensional adiabatic potential surfaces corresponding to the various electronic states of the solvated molecular ion, and the eigenvalue gradients prescribe the classical forces needed to propagate the trajectory; nonadiabatic transitions are treated using a stochastic surface-hopping algorithm.[60−66]

The two models differ in how the Hamiltonian matrix is constructed. Coker and co-workers assemble the solute−solvent interactions using the Diatomics-in-Ionic-Systems prescription of Last and George,[67] which augments the well-known Diatomics-in-molecules method with terms that account for polarization of neutral fragments by charged ones. The solute electronic wave functions are written as linear combinations of localized atomic basis functions, and the charge distribution corresponding to each basis function is approximated by a single point charge at the I^- nucleus. By modulating the energies of these localized basis states, the solvent manipulates their contributions to the wave function and thus induces charge flow within the solute. Our group starts with ab initio calculations of the electronic structure of the isolated solute,[68] from which we extract the one electron density matrix in the form of a distributed multipole expansion.[69] Since the response of the solute electronic structure to any one-electron operator can be computed from this density matrix, we can express the electrostatic and induction interactions between solute and solvent in terms of the interactions between charge and polarization centers on the solvent molecules and the distributed multipole operators of the solute.[58,59] In the basis defined by the electronic states of the isolated solute, the diagonal elements of the distributed multipole operators describe the charge distribution in the various solute states, while the off-diagonal terms describe transition charge distributions that account for the polarization of the solute wave function by the solvent. The remaining dispersion and repulsion terms are described by empirical short-range potentials with parameters taken from high-resolution photoelectron spectra.[70] A detailed description of this model has been published elsewhere.[59]

Molecular dynamics simulations based on these models have succeeded in reproducing the basic trends in the experimental product distributions,[53,55,56,59,71] the time-resolved photoelectron spectra,[57] and the transient absorption recovery.[54,72] Recently, the simulations have made successful predictions as well: the rapid electronic quenching following UV excitation of large $I_2^-(CO_2)_n$ clusters was seen in the simulations[71] before it was confirmed by experiment.[10] It is fair to say that simulations now play an equal role with experiment in unravelling the complex dynamics of these systems.

II. Charge Flow in Solvated Dihalide Anions

Normal and Anomalous Charge Flow. When a molecular ion is embedded in a cluster, a liquid solution, or a solid matrix, the ionic charge cloud becomes polarized. The magnitude of this polarization can be very complicated to calculate since the solute electrons interact strongly with each other as well as with the electric fields produced by the surrounding solvent molecules. Fortunately, dihalides behave much more simply than the general case. These molecules have a valence electron configuration corresponding to a single hole in a closed shell, and to a first approximation such configurations are isomorphic to one-electron systems.[45] We can thus go a long way toward understanding the flow of charge in solvated I_2^- or ICl^- by considering the response of a one-electron diatomic molecule to an external electric field. The straightforward procedures required to recast these results for one-hole configurations have been described elsewhere.[40]

Let us begin with the isolated solute molecule in its electronic ground state, with the nuclei near their equilibrium bond distance, R_e. The electron resides in a bonding molecular orbital, and the corresponding electronic charge distribution is symmetrically shared between the two equivalent atoms. To photodissociate the molecule, we promote the electron to an antibonding orbital. In this excited state the charge is still equally shared by the atoms, although there is less charge density in

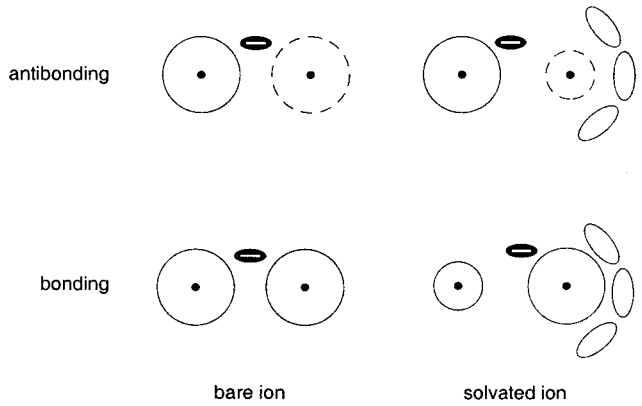

Figure 2. Anomalous charge flow in a diatomic molecular ion. In the bare ion the charge is shared equally between the two nuclei in both bonding and antibonding states. When solvation is asymmetric, the charge localizes on the more solvated atom in the ground electronic state, leaving less charge density on this atom in the excited state.

the region between them. As the molecule dissociates, the wave function evolves into a superposition of disjoint localized pieces, one centered on each atom, representing the equal probabilities of finding the charge on either one when a measurement is made.

This description must be revised when the molecule is immersed in a solvent. Since highly extended superposition states are notoriously sensitive to external perturbations, one expects that even a slight asymmetry in the solvent environment will localize the charge distribution as the molecule dissociates. Put another way, at large R the bonding and antibonding molecular states become nearly degenerate and are easily mixed by solvent perturbations. This solvent-induced localization will take place when the energetic asymmetry between the atoms, created by the solvent environment, exceeds the resonance electronic coupling between them. Using the energy gap between bonding and antibonding states in the isolated molecule as a measure of the electronic coupling, we infer that at small and intermediate distances the charge distribution will be mostly delocalized whereas at large distances it will be localized.[18,41,47]

Given that the solvent forces the charge distribution to localize, we next ask *where* it localizes—which of the two atoms gets the charge when the molecule dissociates? One might guess that the electron settles on the atom whose environment is more favorably disposed to solvate a charge, since this choice leads to a lower electronic energy for the system. This is indeed what happens during thermal dissociation in the electronic ground state, but photodissociation actually leads to the opposite result: the charge moves to the *less* solvated atom. This "anomalous charge flow", as we have called it, can be understood using a molecular orbital argument devised by Papanikolas[29,40,41] and illustrated in Figure 2.[73] The left-hand panel shows the bonding and antibonding molecular orbitals of an isolated homonuclear diatomic molecule. In the right-hand panel, the symmetry has been broken by adding solvent molecules to one side. The ground-state wave function distorts so that more amplitude resides on the more solvated right-hand atom, giving rise to a charge distribution that is polarized toward the solvent. Since the excited-state wave function must remain orthogonal to that of the ground state, its wave function must distort in the opposite direction, so the charge flows away from the solvent.

The flow of charge toward a higher-energy site, in response to the electric field generated by the solvent, implies that the parallel component of the molecular polarizability tensor must be negative. From the familiar perturbation-theory expression for the polarizability α_n of a state $|n\rangle$ in terms of the energies of the states and the dipole moment matrix elements connecting them,[69]

$$\alpha_n = 2\sum_{n'} \frac{|\langle n|\mu|n'\rangle|^2}{[E_{n'} - E_n]} \qquad (1)$$

one can infer that α_n must be positive in the ground state but *may* be negative in an excited state that is strongly coupled to states below it. For a two-state system, such as illustrated in Figure 2, the ground and excited-state polarizabilities are equal in magnitude and opposite in sign. In a general multistate system the excited-state polarizability will be negative if the negative contributions from the lower states outweigh the positive contributions from higher states. Examples of this behavior have been noted in atomic physics—perhaps the simplest is the 2^1P-(1s2p) state of the He atom, which is strongly coupled to the nearby 2^1S(1s2s) state[74,75]—but it appears to have received little attention in molecular and chemical physics.

Although the preceding discussion is couched in terms of a very simple one-electron model, more sophisticated semiempirical treatments[40] and high-level ab initio calculations[68] show that the general conclusions continue to hold in realistic models of dihalide electronic structure. Spin−orbit coupling complicates the picture by mixing together states of bonding and antibonding character,[40,68] but the correlation between anomalous charge flow and antibonding character still applies. Unfortunately, this simple rule appears to hold only for molecules whose electronic structure is dominated by single-electron or single-hole configurations. In the hydrogen molecule, for example, the first excited state ($^3\Sigma_u$) is purely repulsive, but it must have a positive polarizability since it is the lowest electronic state having triplet spin character and there are no dipole matrix elements coupling it to the singlet ground state. Nevertheless, the observation that polarizabilities are in fact negative in a wide class of excited electronic states suggests that this unusual behavior deserves attention in more complex systems as well.

Charge Flow and Caging. A remarkable property of these systems, first seen in the experiments more than a decade ago, is the very high caging efficiency. In the near-IR photodissociation of $I_2^-(CO_2)_n$, for example, both experiment and simulation find that the probability of recombination reaches 100% for a single solvent shell around the ion, and that clusters comprising less than half of a solvent shell induce recombination as much as 50% of the time (Figure 3). Anomalous charge flow provides an appealing rationale for these results. Immediately after photoexcitation, the charge moves toward the less solvated atom, so that photodissociation begins with an attempt to eject an I^- ion from the cluster. The escape of this ion is inhibited by its long-range couloumbic attraction to the rest of the cluster, giving rise to recombination in the absence of a physical "cage" around the solute.

An examination of the simulations confirms this picture. In our simulation of $I_2^-(CO_2)_n$ photodissociation at 790 nm, trajectories never dissociate on the initially excited A′ state because the long-range attractive forces that act in this "anomalous" state are too strong.[56] Instead, dissociation only occurs after a nonadiabatic transition to an electronic state characterized by "normal" charge flow. These transitions occur by two mechanisms: "charge transfer", in which the excess electron on the nascent I^- ion hops back to the other I atom, and "solvent transfer", in which the charge stays fixed while the solvent molecules move so as to catch it.[54,59] Both mechanisms result in solvated iodide ions, and serve to convert the electronic

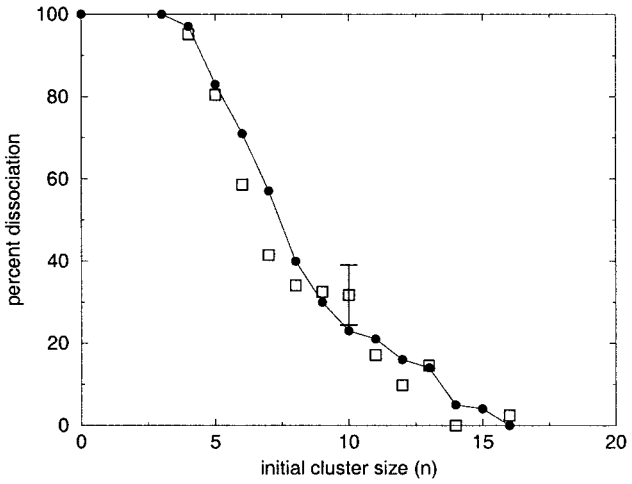

Figure 3. Branching ratio for the products of $I_2^-(CO_2)_n$ photodissociation at 790 nm. The filled circles are the experimental data and the squares show the simulation results. The 1σ error bar shown for $n = 10$ is based on the statistical sampling and is representative of the error bars at other cluster sizes.

energy of the solute into kinetic energy of the solvent. In the $I_2^-Ar_n$ clusters, in contrast, the long-range forces between I^- and the residual cluster are weaker, so that I^- ions can sometimes escape on the A′ potential curve, giving rise to a bimodal structure in the mass spectrum of the dissociated products as discussed in the next section. As a result, dissociation is more likely and recombination is not seen in clusters having less than half a solvent shell.[53,55]

We can now understand why the pioneering simulations of Perera and Amar,[38] which treated both charge-localization and electronic transitions in an ad-hoc fashion, were able to reproduce the experimental caging fraction. Perera and Amar arbitrarily forced the charge distribution to localize at a particular solute bond distance, irrespective of the state of the solvent, and selected the atom which was to receive the electron at random. Once this choice was made, the charge remained on that atom until (and unless) recombination took place, when it was forced to delocalize again. As a result, in half of the simulation trajectories the charge ended up in the "anomalous" location, on the less solvated atom, and subsequently experienced the long-range forces that pull the solute together again. This roughly mimics the results of the self-consistent simulations, in which the charge always begins by moving away from the cluster but may later end up becoming solvated after a nonadiabatic transition, so that after about one picosecond both normal and anomalous configurations are found in the ensemble.

Ion Ejection. The experimental caging fraction is obtained from the mass spectra of the recombined photoproducts. Complementary information about the dissociation dynamics can be obtained from the mass spectra of the *dissociated* products, which reveal how many solvent molecules remain attached to the I^- ion when it reaches the mass detector. In an experimental study of the 790 nm photodissociation of $I_2^-Ar_n$ clusters, Vorsa et al.[27] found that the distribution of I^--based products was distinctly bimodal. In the low-mass product mode, I^- arrived at the detector accompanied by 0, 1, or (rarely) 2 Ar atoms, irrespective of the size of the precursor cluster. In the high-mass mode, in contrast, the number of atoms attached to the ion was much larger and scaled linearly with the size of the precursor cluster. The simulations reproduce these trends qualitatively,[55] although the simulated product distributions are shifted to higher mass, presumably because the simulations are terminated after 50−200 ps while the experimental products are measured on a time scale of microseconds.

Initially it was thought that the two product modes might arise from different types of initial cluster structures, but an examination of the simulations suggests that they actually reflect two different dissociation mechanisms. Figure 4 shows three typical trajectories from a simulation of the photodissociation of $I_2^-Ar_{13}$. During the first 100 fs after excitation, the anion charge localizes on the I atom that is leaving the cluster, in accordance with anomalous charge flow. In the left-hand panel this ion ejection succeeds, and the departing ion strips off an Ar atom to form a low-mass product. In the middle panel the Ar cluster captures the ion ("solvent transfer"), while a neutral I atom falls out the backside, giving rise to high-mass products. Finally, in the right-hand panel the failure of ion ejection is followed by recombination and subsequent delocalization of the charge. Further support for this view comes from the femtosecond time-resolved photoelectron spectra (FPES) of Neumark and co-workers,[11,14,15,57] which probe the local environment of the excess electron directly. By combining the FPES with time-independent threshold photodetachment measurements,[70] Greenblatt et al.[14] have estimated the average number of Ar atoms that surround the I^- ion during the dissociation process. Their results are consistent with our prediction that the charge resides on the less solvated atom.

These simple examples show that by classifying the solute electronic states as "normal" or "anomalous" with respect to solvent-induced charge flow we can achieve insight into the short-time dynamics that immediately follows dissociation. At longer times, however, nonadiabatic transitions force us to consider the dynamics on multiple potential energy surfaces. A more complete description of the solute electronic states and their response to solvent perturbations is then required. In the next section we construct such a description by recasting these ideas in the language of electron transfer theory.

III. Electron-Transfer Perspective

The preceding discussion brought out the importance of *solvent asymmetry*, or inhomogeneity in the local environment surrounding the solute anion. An asymmetric solvent favors a compact, localized charge distribution, and thus acts in opposition to the chemical bonding forces within the solute which tend to delocalize the charge. This competition between localizing and delocalizing interactions also plays a central role in the theory of electron-transfer reactions in solution,[43−45] and that theory provides us with a convenient way to quantify the concept of solvent asymmetry. Our approach to this problem builds on the work of Hynes, Barbara, Benjamin, and co-workers[17−19,47−50] who showed that the recombination of I_2^- on the electronic ground state could be viewed as a special type of electron transfer process, in which the system evolves smoothly between the limits of weak and strong electronic coupling as the atoms come together. In this section we show that by extending this approach so as to incorporate electronic excited states, we can provide a comprehensive physical picture of the dynamics that follow photoexcitation.

A Two-State Model. In the theory of electron transfer reactions, one usually begins with "donor" and "acceptor" sites immersed in a polarizable medium. The charge hops from donor to acceptor at a rate that depends on the local energies of the two sites and on the strength of the electronic coupling between them. At the beginning of the reaction the solvent stabilizes the charge on the donor, and transfer of the electron is accompanied by reorganization of the solvent into a configu-

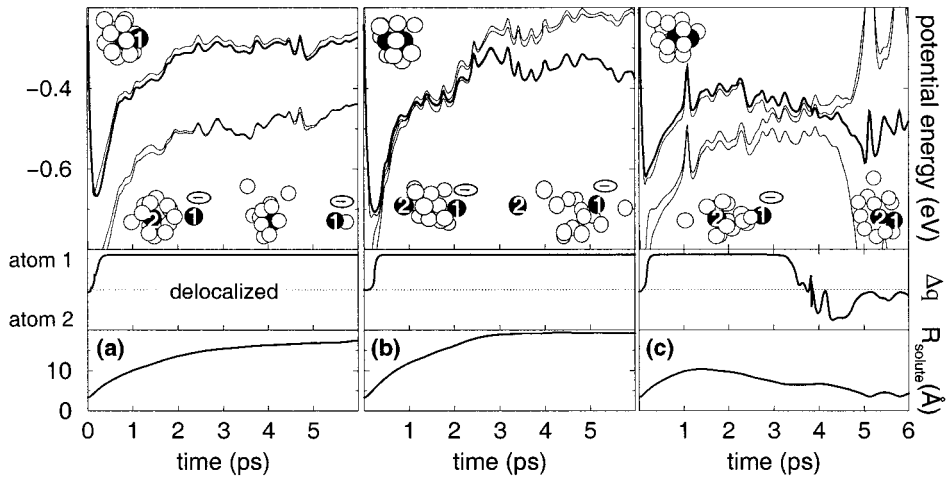

Figure 4. Photodissociation of $I_2^-Ar_{13}$. The adiabatic energies, the location of the charge (Δq), and the I−I distance are plotted as a function of time. The heavier line in the top panel shows the energy of the currently occupied state. Snapshots of the configurations showing the localization of the charge are shown at $t = 0$, 1, and 5 ps. (a) shows a dissociative trajectory which forms I^-Ar_1 and $I{\cdot}Ar_9$ as a direct result of the anomalous charge flow. (b) shows a dissociative trajectory which forms I^-Ar_7 and I following solvent transfer from atom 2 to atom 1 during the first few ps. (c) shows a trajectory which recombines in the excited electronic state ultimately forming $I_2^-Ar_5$.

ration that favors the acceptor. The reaction coordinate for this process thus lies within the solvent.[43,44] Most applications of electron transfer theory deal with polar solvents, for which the solvent coordinate is conveniently expressed in terms of the orientational polarization. Since we are interested in nonpolar solvents such as Ar and CO_2, for which this quantity vanishes, we instead define the solvent coordinate in terms of the electrostatic potential difference $\Delta\Phi$ between the donor and the acceptor sites. Explicitly, $\Delta\Phi$ for a particular solvent configuration is calculated by measuring the change in energy when a charge of $-e$ is moved from donor to acceptor, holding all nuclear coordinates fixed. The magnitude of $\Delta\Phi$ is small when the solvent molecules are nearly equally shared between the two sites (a "symmetric" cluster) and large when one site is preferentially solvated (an "asymmetric" cluster). For polar solvents, this prescription reduces to the traditional one when only charge−dipole interactions are included; motion along the solvent coordinate consists primarily of reorientation of the permanent dipoles on the solvent molecules. For nonpolar solvents, we find that the molecular motions that contribute to $\Delta\Phi$ are different: in Ar, a large change in $\Delta\Phi$ arises from the overall motion of the solvent cage from one site to the other, while in CO_2 both translational and orientational motions are involved. These differences on the molecular scale should be kept in mind when drawing analogies between the cluster experiments and solution phase electron transfer.

Let us now consider how the electronic energy of the donor−acceptor system depends on our solvent coordinate. At large internuclear distances it is convenient to use a diabatic representation, in which the electronic coupling is neglected,[45] so that the electronic charge distribution stays fixed as the solvent molecules move. If we sketch the energies of the diabatic states as a function of $\Delta\Phi$, we obtain a pair of "Marcus parabolas" corresponding to an electron localized on either site; in the case of a symmetric D−A system, such as I_2^-, the parabolas are equivalent and cross at $\Delta\Phi = 0$. At the minimum of a Marcus parabola, the solvent is equilibrated to a localized charge, and as the solvent fluctuates, $\Delta\Phi$ oscillates around the minimum. When we restore the electronic coupling, the diabatic curves are transformed into adiabatic curves having an avoided crossing at $\Delta\Phi = 0$, and the energy gap at the crossing is proportional to the strength of the coupling. In the weak-coupling limit the lower adiabat forms a double well whose minima closely

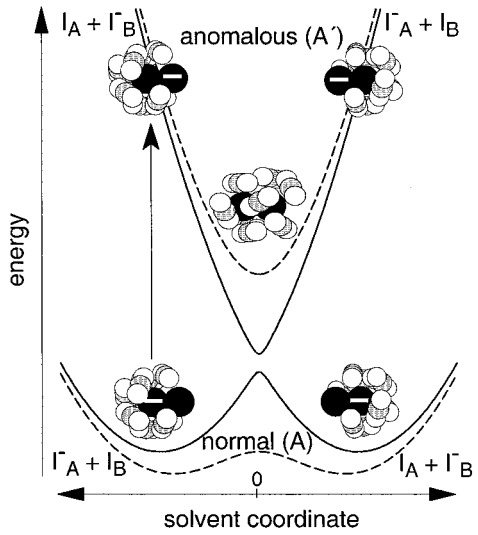

Figure 5. Schematic potential energy curves for a two-state model of a solvated diatomic molecular ion. The dashed curves represent a cross-section at small internuclear distances, where the electronic coupling is strong compared to the solute−solvent interactions. The solid curves represent the limit of weak electronic coupling, which is appropriate at long bond lengths. Anomalous charge flow in the upper state is illustrated by the cluster snapshots.

resemble the original diabatic wells, while the upper adiabat forms a single well. For sufficiently strong electronic coupling the barrier on the lower adiabat is obliterated and it, too, forms a single well.

Now consider the behavior of the electronic charge distribution as the system moves along the adiabatic curves in Figure 5. On the lower adiabat, charge and solvent move in phase with each other. As the solvent coordinate changes sign, the system crosses the barrier and the electronic wave function smoothly transforms from one localized on I_A to one localized on I_B, in accord with the traditional picture of adiabatic electron transfer. But now consider what happens during adiabatic motion on the *upper* curve. Since the left-hand limb of the upper adiabat arose from the diabatic curve whose minimum is on the right, and vice versa, the charge and solvent must be moving in opposite directions! (One can also see this by realizing that a Franck−Condon optical excitation from the lower to the upper adiabat corresponds to a charge-transfer transition.) This is precisely

the phenomenon of "anomalous charge flow", or negative electronic polarizability, derived in section II from a molecular orbital picture of the solute electronic structure.

The two-state Marcus picture also provides a simple way to understand how anomalous charge flow reverts to normal charge flow following a nonadiabatic electronic transition. At short bond distances R, the anomalous and normal states are well separated, while at large R and small $\Delta\Phi$ they come close together. We thus expect nonadiabatic transitions to occur with high probability if the solvent approaches a symmetric geometry while the nuclei are far apart, and we can use the picture to characterize the two mechanisms for nonadiabatic transitions that were observed in the simulations. A simple diabatic passage through the crossing region, in which the system hops from the upper to the lower adiabat as $\Delta\Phi$ passes monotonically through zero, corresponds to a "solvent transfer" event, in which the charge distribution stays fixed while the solvent moves toward the charge. In a nonadiabatic charge-transfer event, in contrast, the charge switches from one atom to the other as the solvent coordinate approaches zero, and the solvent then reverses direction. Both mechanisms lead to a charge distribution that is stabilized by the solvent on the lower state. In heterogeneous systems such as ICl^-, the two mechanisms can be distinguished since they lead to different products.[73,76]

Multistate Models. In the two state model, an electron is transferred between two localized atomic orbitals. As discussed in section II, a dihalide anion, with one hole in a closed valence shell, behaves much like a one-electron diatomic molecule. Since the hole may reside in any one of the three degenerate p orbitals on either atom, however, we need to expand the state space in order to fully describe the valence excited states.

As before, let us start with the two sites far apart, and let us also neglect the spin−orbit interaction for the time being. Since the three p orbitals on an isolated atom are equivalent, we get three degenerate pairs of Marcus parabolas in the diabatic representation. When we bring the atoms together the atomic orbitals overlap and each pair of diabats gives rise to a "normal", double-welled lower adiabat and an "anomalous", single-welled upper adiabat. Since the overlap between orbitals that point along the internuclear axis (the p_Σ orbitals) is larger than the overlap between orbitals parallel to the axis (the p_Π orbitals), the 3-fold degeneracy among the diabats will be partially lifted in the adiabatic representation, and the Σ-adiabats will have a larger energy gap at $\Delta\Phi = 0$ (corresponding to a stronger electronic coupling) than the Π-adiabats. We thus end up with four distinct adiabatic curves, two of which are doubly degenerate, giving a total of six states (Figure 6. We refer to this as the "Case (a) picture", since it corresponds to the Hund's Case (a) coupling scheme for the electronic states of the isolated molecule.

To complete the picture we need to restore the spin−orbit coupling, which mixes states of Σ and Π character and removes the degeneracy in the Case (a) adiabatic curves. Since the atomic spin−orbit energy of I is very large (0.94 eV), it is convenient to couple the spin and angular momenta on individual atoms, giving localized basis functions corresponding to I in its ground state ($^2P_{1/2}$) and to spin−orbit excited I, or I* ($^2P_{3/2}$). When I_2^- is immersed in a solvent, and the atoms pulled far apart so that the electronic coupling between them is very small, we get two degenerate pairs of diabatic Marcus parabolas that correspond to $I^- + I$, and one nondegenerate pair corresponding to $I^- + I^*$. As the atoms are brought closer, each pair of diabats again produces a pair of adiabats, in which the lower curve shows normal charge flow and the upper shows anomalous charge flow.

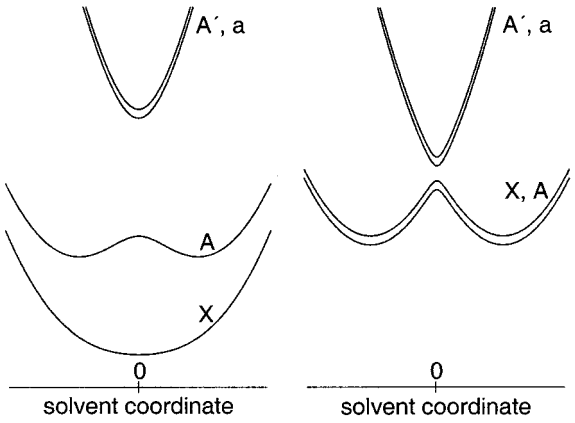

Figure 6. Effect of solvation on dihalide electronic structure, neglecting spin−orbit coupling (Hund's Case (a)). Left hand panel: adiabatic curves at small internuclear distance R (strong electronic coupling). Right-hand panel: adiabatic curves at large R (weak electronic coupling.) In Case (a) the A and A′ curves are doubly degenerate.

As in the Case (a) analysis, the degeneracy in the diabatic representation is lifted in the adiabatic representation because different pairs of diabats are coupled by different electronic matrix elements, reflecting the differing degree of overlap between respective pairs of atomic basis functions.[77] One then gets six distinct adiabatic curves in the Case (c) representation, each of which may be correlated to an electronic state of the isolated I_2^- molecule.[78]

Putting the pieces together, we arrive at the schematic potential energy curves for solvated I_2^- depicted in Figure 7. In the left-hand panel we show the diabatic curves. In addition to the previously discussed crossings at $\Delta\Phi = 0$, which are associated with conventional electron transfer, we see crossings between diabats arising from different spin−orbit states. These crossings, which occur when the solvent coordinate is equal to the atomic spin−orbit energy, lead to efficient electronic quenching in the solvated ion.[40,71] In the right-hand panel we show the adiabatic curves that arise when pairs of diabatic curves are mixed.[79] The X, A, and a′ states of I_2^- correspond to normal charge flow adiabats, whereas the A′, a, and B states correspond to anomalous charge flow adiabats, precisely as one would guess from the bonding or antibonding character (presence or absence of wells in the isolated molecule potential curves) of the states (Figure 1). We also see that for small and intermediate values of $\Delta\Phi$, the four lower curves in Figure 7 have the same qualitative shape as the Case (a) curves in Figure 6. Thus, if one is only interested in dynamics on these lower states, the primary effect of the spin−orbit coupling to reduce the size of the effective state space by pushing two of the six states up to very high energy. We can thus use Figure 6, with all curves regarded as nondegenerate, to understand most aspects of the 790 nm excitation experiments, which prepare the system on the A′ state. In contrast, all six states must be included in the analysis of the UV experiments, in which the system is prepared on the B state.

IV. Applying the Electron-Transfer Picture: Photodissociation of $I_2^-(CO_2)_n$

Thus far, we have described the qualitative shapes of the two-dimensional effective potential surfaces that specify the electronic energy as a function of the solute bond length R and the solvent asymmetry coordinate $\Delta\Phi$, but we have not given any prescription for calculating them. For example, we have not given an expression for the curvature of the diabatic wells in

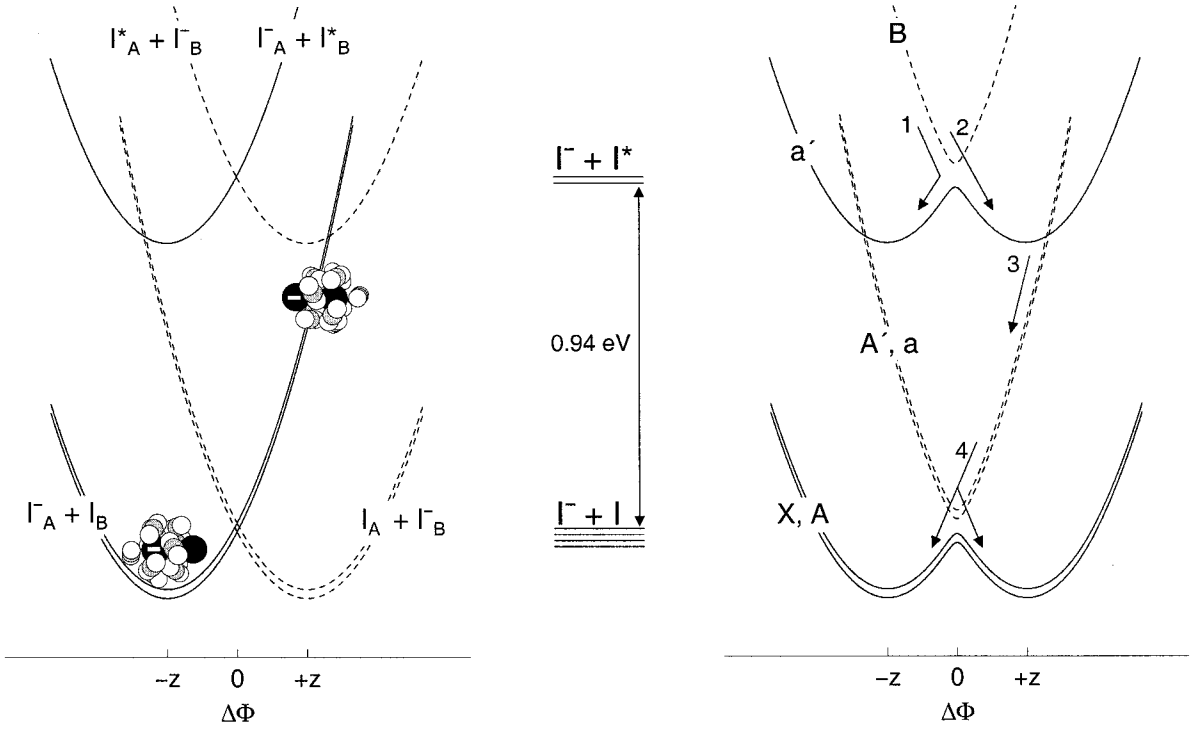

Figure 7. Effect of solvation on dihalide electronic structure at intermediate to long bond lengths, in the limit of large spin−orbit coupling (Hund's Case (c)). Center: energy levels of isolated $I^- + I$ in its two lowest electronic states. Left hand panel: diabatic energy vs solvent coordinate, $\Delta\Phi$. Right-hand panel: adiabatic states associated with molecular state labels of I_2^-. States B, A′ and a exhibit anomalous charge flow. Arrows depict relaxation pathways observed in trajectories.

Figure 7; indeed, we do not even know over what range of $\Delta\Phi$ these curves are accurately represented by parabolas. The simplest versions of Marcus theory provide analytical formulas for these quantities, but these derive from a dielectric continuum description of the solvent which is not appropriate for our systems. In principle we could calculate free energy surfaces for the solvated ion, by carrying out Monte Carlo or equilibrium molecular dynamics simulations in which R and $\Delta\Phi$ are constrained while the microscopic degrees of freedom are averaged over. In practice it is easier to plot trajectory ensembles in the (R, $\Delta\Phi$) plane, and to use the patterns that emerge from these figures to infer the shapes of the effective potentials that determine the dynamics.

Near-IR Photodissociation: Solvent Dynamics on Multiple Potential Surfaces. In Figure 8 we plot trajectory ensembles for the photodissociation of I_2^- clustered with 16 and with 9 CO_2 molecules, following excitation at 790 nm. Since 16 CO_2 molecules form a closed shell around I_2^-, the initial solvent environment is nearly symmetric, and the ensemble averaged value of $|\Delta\Phi|$ is about 100 meV. In contrast, at $n = 9$ $|\Delta\Phi|\rangle$ exceeds 600 meV, corresponding to highly asymmetric, open-shelled structures. The three panels shown for each cluster size partition the trajectories based on electronic state. All trajectories begin in the A′ state, shown in the top panel, at $R_{solute} = 3.3$ Å. Upon reaching the coupling regions marked with ovals, trajectories make transitions to the lower-lying A and X states, shown on the left and right, respectively. Transitions between these two lower states can also occur in the regions outlined with rectangles.

Before discussing the dynamics in detail, we point out some large-scale features in Figure 8. Trajectories fill out differently shaped regions regions on the three electronic states. On the A state, they are concentrated at large values of R and $|\Delta\Phi|$. On the X state, they form a horseshoe profile in which $|\Delta\Phi|$ is large when R is large, but small when R is near the equilibrium internuclear distance. On the A′ state, they occupy different regions for the two cluster sizes: for $n = 16$ they lie in a narrow strip near $|\Delta\Phi| = 0$, whereas for $n = 9$ they pass from large to small $|\Delta\Phi|$ as they move out to large R. These patterns can be understood with reference to the Marcus curves in Figure 7. Both X and A states show "normal" charge flow, so a cross-section through their potential surfaces at large R forms a double well which confines trajectories to large $|\Delta\Phi|$. The X state reverts to a single well at small R, where the electronic coupling overwhelms the solvation energy. This does not happen in the A state because the electronic coupling is much weaker—instead one finds "solvent-separated pairs" consisting of an I^- ion bound to several CO_2 molecules and an I atom. Since the A′ state shows anomalous charge flow, it has a single well in the solvent coordinate. For $n = 16$, $|\Delta\Phi|$ starts out small since the initial cluster geometries are nearly symmetric, and remains small until the trajectories hop to another state. For $n = 9$, the initial values of $\Delta\Phi$ span a much larger range, but trajectories that start with large $|\Delta\Phi|$ are quickly focused in to small $|\Delta\Phi|$ at large R.

With these patterns in mind, we can sketch the history of the ensembles. After excitation to the A′ state, trajectories are funneled in toward the minimum at $|\Delta\Phi| = 0$ as they move outward in R. The long-range attraction between the departing I^- and the residual cluster prevents direct dissociation on this anomalous state, so trajectories hop to the normal A and X states, where they find themselves on top of a potential ridge. They then rush out to large $|\Delta\Phi|$, as the solvent pursues the localizing charge. Trajectories on the A state form solvent-separated pairs which either dissociate by thermal evaporation of I, or hop to the X state. Trajectories on the X state lose energy through vibrational relaxation, and eventually reach the strong electronic coupling regime where the charge distribution becomes delocalized again while the solvent adopts a symmetric configuration.

UV Photodissociation: Spin−orbit Quenching via Solvent-

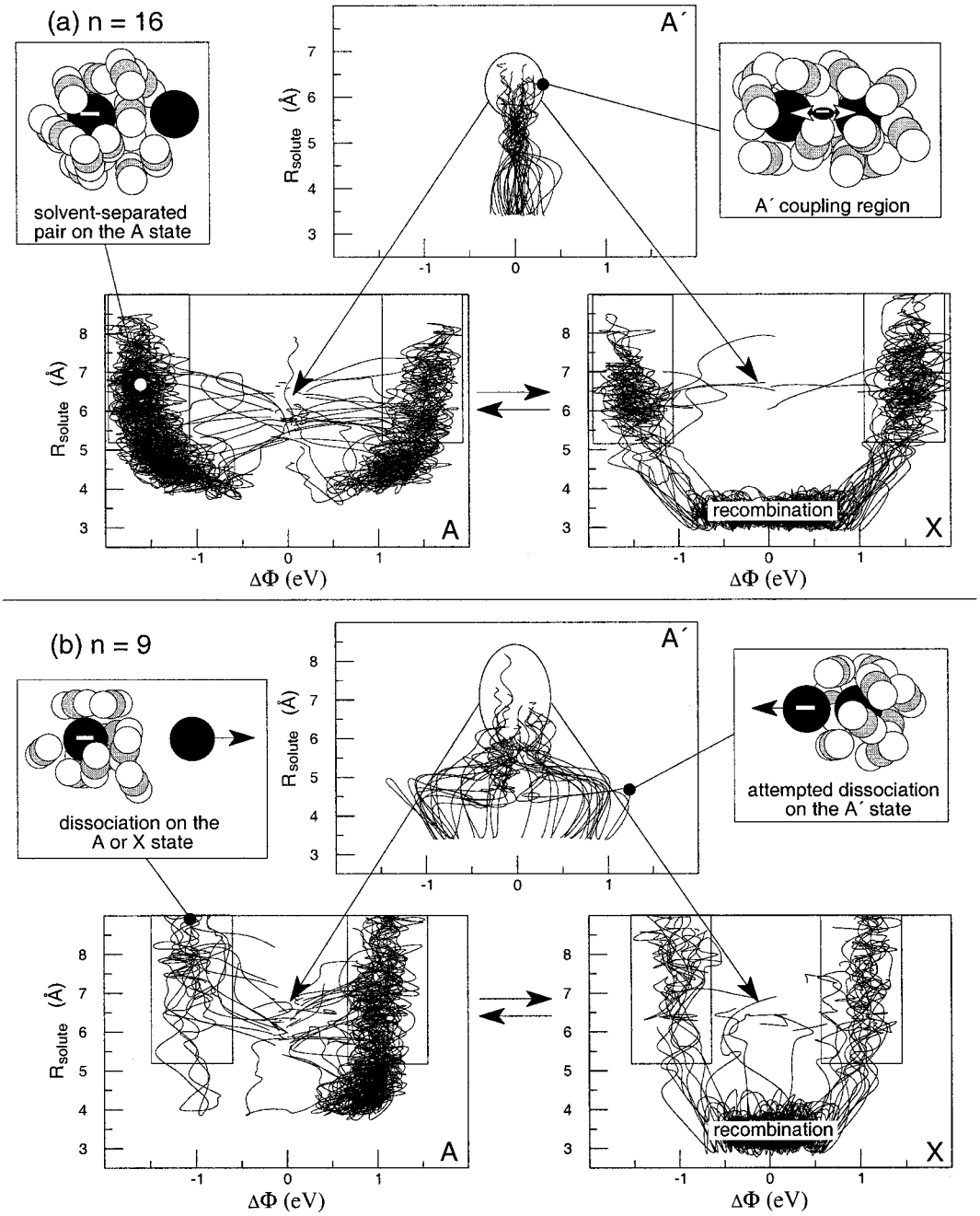

Figure 8. Dynamics of an ensemble of 41 trajectories projected onto the solute bond length and the solvent coordinate for $n = 16$ (a) and $n = 9$ (b). Trajectories begin in the A′ state at $R_{solute} = 3.3$ Å and undergo transitions to the lower states in the regions indicated with ovals. A ↔ X coupling regions are marked with rectangles. The apparent favoring of the right side of the A state in (b) is due to the few trajectories that remain trapped for a long time.

mediated Electron Transfer. The electron-transfer perspective gives us an attractive physical picture with which to interpret the results of the near-IR photodissociation experiments. The true measure of the value of a hypothesis, however, is its ability to predict new and unexpected phenomena. Recent experiments on photodissociation of I_2^- in the near UV have enabled us to make and test such a prediction.

Let us return to the potential energy curves in Figure 1. Excitation of I_2^- at 350 nm puts the molecule on the B state, which correlates adiabatically to $I^- + I^*$. The very large energy gap between I and I* leads one to expect little or no nonadiabatic relaxation during UV dissociation of the isolated molecule, and this expectation is confirmed by experiment.[10] Until recently, it was generally believed that electronic relaxation would also be extremely inefficient in I_2^- clustered with CO_2, since the cross section for quenching of I* in gas-phase collisions with CO_2 is extremely small.[80] However, this argument ignores the influence of the solvent on the solute electronic structure. In $I_2^-(CO_2)_n$ clusters the solvation energy is about 0.25 eV per CO_2 molecule, so that energy shifts on the order of one eV are easily achieved, and since "normal" and "anomalous" states move in opposite directions in response to an asymmetric solvation environment, these shifts can bring together electronic states that are very far apart in the isolated molecule. On these grounds, Maslen et al.[40] argued that a solvent-induced resonance between the normal a′ state and the anomalous A′ state could provide a mechanism for efficient spin−orbit quenching in solvated I_2^-.

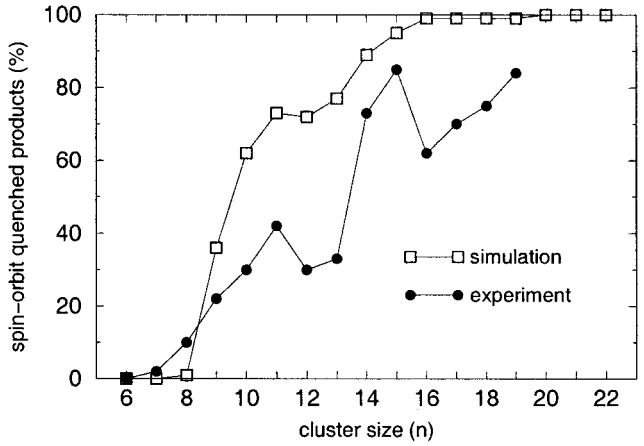

Figure 9. Probability of spin−orbit quenching following photodissociation of $I_2^-(CO_2)_n$ 350 nm. The quenched products either recombine or dissociate to iodide + ground-state I atoms. The structure in the experimental profile is real and reproducible.

The Marcus curves in Figure 7 provide further insight into the quenching mechanism. The solvent-induced intersection between the a′ and A′ states corresponds, in the diabatic representation, to a point where the difference between the solvation energy of the I^- ion and the I neutral is approximately equal to the atomic spin−orbit energy of I*. A passage through the crossing then corresponds to the resonant transfer of an electron from a solvated I_2^- to an I_A* atom on the outside of the cluster, resulting in I_A^- on the outside and I_B in its electronic ground state on the inside. After charge transfer the solute finds itself in an extremely unfavorable solvation environment—the electronic energy has been converted into solvent potential energy—and the cluster quickly evaporates several CO_2 molecules as the solvent tries to reorganize. One can also infer from Figure 7 that there should be a *threshold* for spin−orbit quenching as a function of cluster size, since in very small clusters there will not be enough solvent available to bring $\Delta\Phi$ into the neighborhood of 1 eV.

To quantify these predictions, we turn to the simulations. Figure 9 shows our calculated spin−orbit quenching probabilities, together with the experimental results of Sanov et al.[10] Both simulation and experiment display a sharp threshold near $n = 8$. For larger n, simulation and experiment follow similar trends although the quantitative discrepancies are larger than for near-IR photodissociation (Figure 3), suggesting that the simulation model is less accurate at higher energies. An extensive analysis of the simulation results in terms of the multistate Marcus picture has been published elsewhere.[71]

Absorption Recovery Experiments: A New Interpretation. For our final illustration, we turn to the time-resolved pump−probe studies of solvated I_2^-, carried out by Lineberger and co-workers in mass-selected clusters and by Barbara and co-workers in the solution phase. In these experiments, a short pulse dissociates the chromophore, and a second, delayed pulse probes for its reappearance as the atoms recombine. While similar in concept, the two sets of experiments differ in significant respects. The cluster experiments use only small solvent molecules such as Ar, CO_2, and OCS, and are carried out at temperatures of about 60 K, whereas the liquid-phase experiments use larger solvent molecules such as dioxane as well as small ones like water, and are carried out at room temperature. There is also an important difference in the way that the probe absorption is detected: in the solution experiments the attenuation of the transmitted light is measured directly, whereas in the cluster experiments it is inferred from the mass spectrum of the recombined photofragments. If one assumes that all of the energy of an absorbed photon is eventually transferred into the intramolecular degrees of freedom of the solvent, and eventually dissipated by evaporation, a cluster that absorbs both pump and probe photons can evaporate about twice as many solvent molecules as one which absorbs only the pump photon, so the photofragment mass spectrum contains well-defined "one photon" and "two photon" peaks. Despite these differences, the results of the two sets of experiments are broadly similar: in all solvents except Ar, the probe absorption grows in on a time scale of 10−20 ps, and in some solvents a transient peak occurring at about 2 ps after excitation is superimposed on this rise. In Ar, the overall rise time exceeds 100 ps, and no transient peak is seen.

The overall trend in the probe absorption was attributed by both experimental groups to recombination of I_2^- on the ground electronic state. The 10−20 ps rise time then reflects a composite time scale for the complete process of photodissociation, recombination, electronic relaxation, and vibrational relaxation, yielding I_2^- chromophores near their equilibrium geometry. This interpretation has been confirmed by the FPES experiments[13,15] and by simulations.[54] The rise time is much longer in the Ar clusters because most of the solvent is lost by evaporation during the recombination and relaxation process, so that vibrational relaxation becomes very slow.[11,14,57] The origin of the 2 ps transient, however, could not be established from the experiments alone. It seemed unlikely that both the overall rise and the transient were due to the same electronic transition, since the time scales were so different, and the Barbara group confirmed this by showing that when the system was dissociated at 790 nm and the absorption recovery monitored in the ultraviolet (i.e., using the X → B transition), the overall rise remained but the transient disappeared. After ruling out several possibilities on the basis of the polarization dependence of the signal, Papanikolas et al.[6] concluded that the transient peak was due to absorption from the A state to the a state. In this view, the transient arises when a portion of the photodissociation ensemble recombines on the A state, producing a wave packet that absorbs when it reaches the inner turning point. Subsequent experiments[11,13−15] and simulations[53−57,59] demonstrated that A-state recombination did indeed take place, but a closer examination of the simulations revealed that the dynamics on this state was diffusive rather than coherent, with trajectories spreading out over a wide range of solvent and solute configurations rather than forming a tight bundle moving toward the inner wall. Moreover, the energy gap between the A and a states along the simulation trajectories was always much smaller than the energy of the 720 nm probe photon. Thus, while the A state was populated, this did not seem to provide a plausible origin for the 2 ps absorption peak.

We have recently proposed[72,81] that the transient peak is due to absorption from highly excited vibrational states of the ground electronic state to the spin−orbit excited a′ and B states. This possibility had been considered by Papanikolas et al.[6,29] but tentatively ruled out on the grounds that absorption into these states would not yield the observed two-photon fragments, since no mechanism was known that could quench the spin−orbit excitation energy in the a′ and B states into the intracluster modes. The subsequent discovery that spin−orbit quenching is actually highly efficient led us to reexamine this alternative assignment of the probe transition, and using large-scale molecular dynamics simulations we were able to provide compelling evidence for it.[72] Figure 10 compares our simulated absorption recovery signal with the experiments of Papanikolas

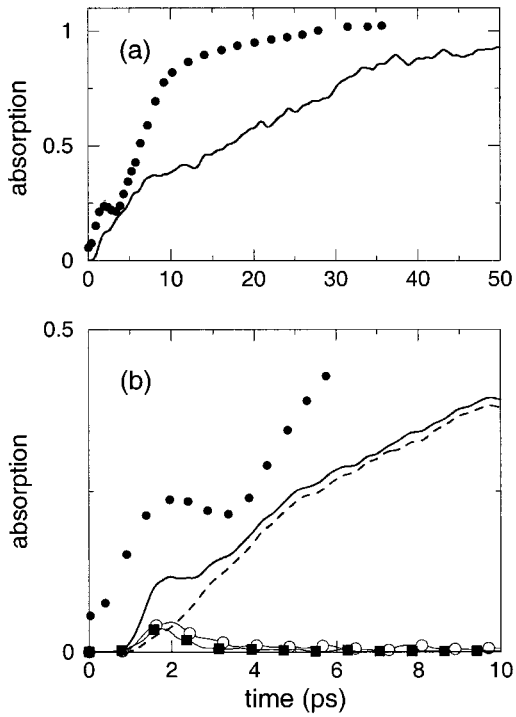

Figure 10. Absorption recovery of $I_2^-CO_{16}$. (a) Comparison of experimental (dots) and simulated (line) signals. Simulated signal is from 100-trajectory ensemble and reaches its asymptotic value between 60 and 80 ps. (b) Solid line is the total simulated signal from a 250-trajectory ensemble, dots are the experimental data. Dashed line is the contribution from the X ↔ A′ transition. The transient feature at 2 ps is due to X → a′ and X → B transitions, shown respectively by the open circles and filled squares.

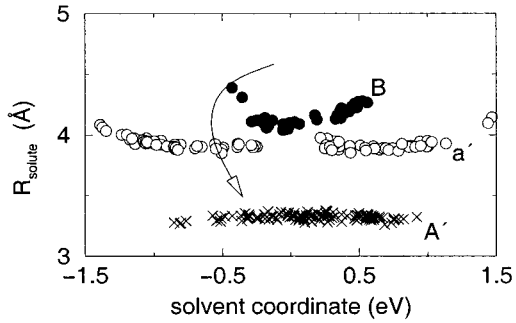

Figure 11. Location of strong, 720 nm absorption regions in the (R, $\Delta\Phi$) plane. Transitions originate on the X state and end on the A′ (x's), a′ (open circles), and B (filled circles) states. Arrow represents simplified pathway for trajectories recombining on the X state.

et al.[6] While the simulation overestimates the rise time for the main absorption recovery, it clearly reproduces the transient absorption feature at 2 ps, and this transient is seen to arise entirely from transitions to the spin−orbit excited states.

This reassignment leads to a new physical picture, in which the transient peak occurs as the I and I^- fragments first begin to recombine, rather than at the inner turning point. The transient thus probes regions of the potential surface in which solvent effects on the solute electronic structure are particularly strong. Once again, the Marcus picture and the associated two-dimensional trajectory maps help us to visualize the experimental consequences of these effects. In Figure 11 we monitor the solute bond length R and the solvent coordinate $\Delta\Phi$ along each trajectory in a photodissociation ensemble, and plot those points for which the contribution to the probe absorption exceeds a threshold value. We see that the X → A′ transitions, which determine the overall absorption recovery, occur near the equilibrium internuclear geometry, in accord with the accepted view that they originate from vibrationally relaxed I_2^-. In contrast, the transitions to the spin−orbit excited states take place at $R \approx 4A$, corresponding to highly vibrationally excited states of I_2^-. The precise location of this absorption window, and thus the shape of the transient, can be adjusted by varying the probe wavelength; this has been seen by Barbara and co-workers,[19] and our simulations provide new insights into the interpretation of those experiments.

Further examination of Figure 11 shows that the two electronic transitions that contribute to the transient peak originate from different regions of solvent configuration space. The shapes of these regions can be understood in terms of two functions of R and $\Delta\Phi$, the energy gap ΔU between the initial and final states, and the transition dipole moment μ that connects them. Let us first consider the energy gap. In the quasiclassical approximation[26,54,82] a trajectory can only contribute to the absorption signal if the energy gap is near to resonance with the probe frequency. The probe absorption regions should thus lie along the curves that satisfy the equation $\Delta U(R, \Delta\Phi) = h\nu$. The a′ and X states both exhibit normal charge flow, so their potential energy surfaces have the characteristic double-well shape shown in Figure 7. Since the two surfaces are roughly parallel, the energy gap depends only weakly on $\Delta\Phi$, so the region of strong X → a′ absorption lies along a horizontal line in the (R, $\Delta\Phi$) plane. In contrast, the B state surface has the single-well shape characteristic of anomalous charge flow. The energy gap between X and B thus depends strongly on $\Delta\Phi$, so it is necessary to vary both R and $\Delta\Phi$ to hold ΔU fixed. Since the gap increases as one moves away from $\Delta\Phi$ at fixed R, and shrinks as one moves to larger R at fixed $\Delta\Phi$, the curves corresponding to fixed ΔU bend outward as seen in Figure 11. The disappearance of the X → a′ transition near $\Delta\Phi = 0$ is a transition dipole effect: in the isolated molecule, or in a perfectly symmetric solvation environment, the X and a′ states both have *ungerade* symmetry so the transition is forbidden. In an asymmetric environment the solute wave functions are polarized, lifting this selection rule, and for large $\Delta\Phi$ the X → a′ and X → B transitions have approximately equal intrinsic intensities.

V. Conclusion

The examples discussed in this article illustrate the crucial role played by solvent-induced charge flow in the photodissociation and recombination of dihalide ions in clusters and in solution. Since the solvent strongly perturbs the solute electronic structure, interpretations of the experiments that are based on the potential energy curves of the isolated solute can lead to a qualitatively inaccurate physical picture. On the other hand, our experience with solvation effects in electronic ground states must be also applied with caution, since not only the magnitude but also the direction of the solvent-induced charge flow is strongly state-dependent. We have found that the electron-transfer perspective, first introduced to clarify the mechanism behind fast vibrational relaxation in the electron ground state,[18,47,49] enables us to construct a comprehensive picture of charge flow and solvent dynamics on the entire manifold of coupled potential energy surfaces. Unusual phenomena such as "anomalous" charge flow and ultrafast spin−orbit quenching receive simple, transparent physical explanations when viewed in this light.

The electron transfer perspective emphasizes the role of asymmetry in the local environment around the polarizable solute, and the Marcus solvent coordinate provides a quantitative measure of this asymmetry. The simple patterns that emerge from the trajectory maps in section IV show that this definition

of a solvent coordinate is a useful one for these systems. There are undoubtedly problems in condensed-phase reaction dynamics for which a different choice will be more appropriate. For this reason we believe that it is important to separate the methods used to simulate the dynamics from the concepts used to interpret them. Ideally, the conceptual model should be as simple as possible, while the simulation model should be as comprehensive as practicable, so that the simulation can be used to test the more severe approximations made in the conceptual model. Of course the simulations themselves rely on approximations, often poorly controlled ones, which must be tested against real experiments in the laboratory.

Both our conceptual models and our simulations rely heavily on two major physical approximations: charge transfer from solute to solvent has been neglected, and the nuclear motions have been treated classically, with electronic state changes described by a stochastic surface hopping algorithm. The first approximation appears to be adequate for this class of systems but may well fail as one moves to more strongly interacting solvents having larger electron affinities. A limited amount of charge transfer can in principle be included in the present approach by constructing appropriate pseudopotentials for the solute−solvent interaction, but extensive charge delocalization into the solvent would require a fundamentally different strategy, since we would no longer be dealing with a solvated molecular anion but rather with a solvated electron. Quantum mechanical treatments of the nuclear motion might at first sight seem unnecessary, since the nuclear masses are so large, the temperatures are fairly high and the experimental energy resolution is limited. However, the problem needs to be addressed, because the surface-hopping methods involve approximations whose validity in multidimensional systems is not fully understood.[66] One popular method for describing the dynamics of a quantum mechanical solute in a dissipative bath is to construct reduced equations of motion for the density matrix of a "primary" subsystem.[83] The quantum dynamics of the primary system is treated explicitly, while the interaction with the bath is described by additional terms that account for dephasing and energy relaxation. These equations may be solved directly[36] or converted into a stochastic simulation algorithm for the primary system wave function.[84] Our classical results imply that caution is required in modeling the present problems in this fashion; for example, one ought not to define the primary subsystem to be the solute anion, since it is strongly coupled to the solvent. However, a larger primary subsystem that consists of the solute together with the solvent asymmetry coordinate would appear to provide a suitable model, although it will be computationally demanding to simulate since the density matrix of a two-degree of freedom system is a very large object.

We close with some remarks on the use of cluster experiments and simulations for elucidating chemical dynamics in complex environments. One frequently hears that clusters are suppose to provide "a bridge between the gas and the condensed phase". One might infer from such statements that the properties of finite clusters should lie between those of isolated molecules and those of extended systems. This often turns out to be true—for example, the ionization potentials and electron affinities of metal clusters both converge to the bulk work function as the cluster size increases. In other respects, however, a cluster is better described as a distinct phase of matter with its own characteristic properties. For example, the asymmetry of the local environment around a solute anion can be much more extreme in a cluster than in a bulk fluid, since in the cluster one can have solvent molecules on one side of the solute and vacuum on the other, so that the solvent coordinate can reach larger values. Clusters can thus provide us with model systems in which some solvation effects are accentuated, rather than diminished, with respect to the condensed phase.

Acknowledgment. The foundations of this work, both conceptual and computational, were laid by our former coworkers, Paul Maslen and John Papanikolas, and they have continued to play a vital role in its development. We have learned a great deal from discussions with many experimentalists and theorists, including Carl Lineberger, Dan Neumark, Paul Barbara, Laurie Butler, Casey Hynes, Branka Ladanyi, David Coker, and Mark Ratner. We are especially grateful to members of the Lineberger group (Andrei Sanov, Sreela Nandi, Todd Sanford, Maria Nadal, and Vasil Vorsa) and of the Neumark group (Jeff Greenblatt and Marty Zanni) for providing us with experimental data well in advance of publication and for stimulating discussions about its interpretation. The research described here was supported by grants PHY-9512150 and CHE-987374 from the National Science Foundation, and by the National Center for Supercomputing Applications (NCSA) under Grant CHE970015N for computing time on the SGI Power ChallengeArray and the SGI CRAY Origin2000 at the NCSA, University of Illinois at Urbana-Champaign.

References and Notes

(1) Hynes, J. T. *Annu. Rev. Phys. Chem.* **1984**, *36*, 573.
(2) Alexander, M.; Levinger, N.; Johnson, M.; Ray, D.; Lineberger, W. *J. Chem. Phys.* **1988**, *88*, 6200.
(3) Ray, D.; Levinger, N.; Papanikolas, J.; Lineberger, W. *J. Chem. Phys.* **1989**, *91*, 6533.
(4) Papanikolas, J.; Gord, J.; Levinger, N.; Ray, D.; Vorsa, V.; Lineberger, W. *J. Phys. Chem.* **1991**, *95*, 8028.
(5) Papanikolas, J.; Vorsa, V.; Nadal, M.; Campagnola, P.; Gord, J.; Lineberger, W. *J. Chem. Phys.* **1992**, *97*, 7002.
(6) Papanikolas, J.; Vorsa, V.; Nadal, M.; Campagnola, P.; Buchenau, H.; Lineberger, W. *J. Chem. Phys.* **1993**, *99*, 8733.
(7) Vorsa, V.; Nandi, S.; Campagnola, P. J.; Larsson, M.; Lineberger, W. C. *J. Chem. Phys.* **1997**, *106*, 1402.
(8) Nandi, S.; Sanov, A.; Delaney, N.; Faeder, J.; Parson, R.; Lineberger, W. C. *J. Phys. Chem. A* **1998**, *102*, 8827.
(9) Sanov, A.; Nandi, S.; Lineberger, W. C. *J. Chem. Phys.* **1998**, *108*, 5155.
(10) Sanov, A.; Sanford, T.; Nandi, S.; Lineberger, W. C. *J. Chem. Phys.* **1999**, *111*, 664.
(11) Greenblatt, B. J.; Zanni, M. T.; Neumark, D. M. *Science* **1997**, *276*, 1675.
(12) Zanni, M. T.; Taylor, T. R.; Greenblatt, B. J.; Soep, B.; Neumark, D. M. *J. Chem. Phys.* **1997**, *107*, 7613.
(13) Greenblatt, B. J.; Zanni, M. T.; Neumark, D. M. *Faraday Discuss.* **1997**, *108*, 101.
(14) Greenblatt, B. J.; Zanni, M. T.; Neumark, D. M. *J. Chem. Phys.* **1999**, *111*, 10566.
(15) Greenblatt, B. J.; Zanni, M. T.; Neumark, D. M. *J. Chem. Phys.* **2000**, *112*, 601.
(16) Johnson, A. E.; Levinger, N. E.; Barbara, P. F. *J. Phys. Chem.* **1992**, *96*, 7841.
(17) Alfano, J.; Kimura, Y.; Walhout, P. K.; Barbara, P. F. *Chem. Phys.* **1993**, *175*, 147.
(18) Kliner, D. A. V.; Alfano, J. C.; Barbara, P. F. *J. Chem. Phys.* **1993**, *98*, 5375.
(19) Walhout, P. K.; Alfano, J. C.; Thakur, K. A. M.; Barbara, P. F. *J. Phys. Chem.* **1995**, *99*, 7568.
(20) Franck, J.; Rabinowitch, E. *Trans. Faraday Soc.* **1934**, *30*, 120.
(21) Zimmerman, J.; Noyes, R. M. *J. Chem. Phys.* **1950**, *21*, 2086.
(22) Chuang, T.; Hoffman, G.; Eisenthal, K. *Chem. Phys. Lett.* **1974**, *25*, 201.
(23) Harris, A. L.; Brown, J. K.; Harris, C. B. *Annu. Rev. Phys. Chem.* **1988**, *39*, 341.
(24) Liu, Q.; Wang, J.-K.; Zewail, A. H. *Nature* **1993**, *364*, 427.
(25) Zadoyan, R.; Li, Z.; Martens, C.; Apkarian, V. *J. Chem. Phys.* **1994**, *101*, 6648.
(26) Batista, V. S.; Coker, D. F. *J. Chem. Phys.* **1997**, *106*, 6923.
(27) Vorsa, V.; Campagnola, P. J.; Nandi, S.; Larsson, M.; Lineberger, W. C. *J. Chem. Phys.* **1996**, *105*, 2298.

(28) Nadal, M. The study of the photodissociation and recombination dynamics of mass-selected cluster ions: Solvent effects on the structure and dynamics of the ionic chromophore. Ph.D. Thesis, University of Colorado, 1996.
(29) Papanikolas, J. M. I_2^- photodissociation and cage recombination dynamics in size-selected $I_2^-(CO_2)_n$ clusters. Ph.D. Thesis, University of Colorado, 1994.
(30) Vorsa, V. Photodissociation dynamics of mass-selected anions and anionic clusters. Ph.D. Thesis, University of Colorado, 1996.
(31) Banin, U.; Waldman, A.; Ruhman, S. *J. Chem. Phys.* **1992**, *96*, 2416.
(32) Banin, U.; Ruhman, S. *J. Chem. Phys.* **1993**, *98*, 4391.
(33) Banin, U.; Ruhman, S. *J. Chem. Phys.* **1993**, *99*, 9318.
(34) Banin, U.; Bartana, A.; Ruhman, S.; Kosloff, R. *J. Chem. Phys.* **1994**, *101*, 8461.
(35) Banin, U.; Kosloff, R.; Ruhman, S. *Chem. Phys.* **1994**, *183*, 289.
(36) Ashkenazi, G.; Banin, U.; Bartana, A.; Kosloff, R.; Ruhman, S. *Adv. Chem. Phys.* **1997**, *100*, 317.
(37) Greenblatt, B. J.; Zanni, M. T.; Neumark, D. M. *Chem. Phys. Lett.* **1996**, *258*, 523.
(38) Perera, L.; Amar, F. G. *J. Chem. Phys.* **1989**, *90*, 7354.
(39) Amar, F. G.; Perera, L. *Z. Phys. D.* **1991**, *20*, 173.
(40) Maslen, P. E.; Papanikolas, J. M.; Faeder, J.; Parson, R.; ONeil, S. V. *J. Chem. Phys.* **1994**, *101*, 5731.
(41) Papanikolas, J. M.; Maslen, P. E.; Parson, R. *J. Chem. Phys.* **1995**, *102*, 2452.
(42) Ladanyi, B. M.; Parson, R. *J. Chem. Phys.* **1997**, *107*, 9326.
(43) Marcus, R. A. *Annu. Rev. Phys. Chem.* **1964**, *15*, 155.
(44) Newton, M. D.; Sutin, N. *Annu. Rev. Phys. Chem.* **1984**, *35*, 437.
(45) Schatz, G. C.; Ratner, M. A. *Quantum Mechanics in Chemistry*; Prentice Hall: Englewood Cliffs, NJ, 1993; Chapter 10.
(46) Benjamin, I.; Whitnell, R. M. *Chem. Phys. Lett.* **1993**, *204*, 45.
(47) Gertner, B. J.; Ando, K.; Bianco, R.; Hynes, J. T. *Chem. Phys.* **1994**, *183*, 309.
(48) Bianco, R.; Hynes, J. T. *J. Chem. Phys.* **1995**, *102*, 7885.
(49) Benjamin, I.; Barbara, P. F.; Gertner, B. J.; Hynes, J. T. *J. Phys. Chem.* **1995**, *99*, 7557.
(50) Kim, H. J.; Hynes, J. T. *J. Chem. Phys.* **1992**, *96*, 5088.
(51) Bianco, R.; Timoneda, J. J. I.; Hynes, J. T. *J. Phys. Chem.* **1994**, *98*, 12103.
(52) Bianco, R.; Hynes, J. T. *J. Chem. Phys.* **1995**, *102*, 7864.
(53) Batista, V. S.; Coker, D. F. *J. Chem. Phys.* **1997**, *106*, 7102.
(54) Margulis, C.; Coker, D. F. *J. Chem. Phys.* **1999**, *110*, 5677.
(55) Faeder, J.; Delaney, N.; Maslen, P. E.; Parson, R. *Chem. Phys. Lett.* **1997**, *270*, 196.
(56) Delaney, N.; Faeder, J.; Maslen, P. E.; Parson, R. *J. Phys. Chem. A* **1997**, *101*, 8147.
(57) Faeder, J.; Parson, R. *J. Chem. Phys.* **1998**, *108*, 3909.
(58) Maslen, P. E.; Faeder, J.; Parson, R. *Mol. Phys.* **1998**, *94*, 693.
(59) Faeder, J.; Delaney, N.; Maslen, P. E.; Parson, R. *Chem. Phys.* **1998**, *239*, 525.
(60) Tully, J. C. *J. Chem. Phys.* **1990**, *93*, 1061.
(61) Webster, F.; Rossky, P.; Friesner, R. *Comput. Phys. Comm.* **1991**, *63*, 494.
(62) Space, B.; Coker, D. *J. Chem. Phys.* **1991**, *94*, 1976.
(63) Hammes-Schiffer, S.; Tully, J. C. *J. Chem. Phys.* **1994**, *101*, 4657.
(64) Coker, D. F. In *Computer Simulation in Chemical Physics*; Allen, M. P.; Tildesley, D. J., Eds.; Kluwer: Dordrecht, 1993; pp 315−377.
(65) Coker, D. F.; Xiao, L. *J. Chem. Phys.* **1995**, *102*, 496.
(66) Hammes-Schiffer, S. *J. Phys. Chem. A* **1998**, *102*, 10444.
(67) Last, I.; George, T. F. *J. Chem. Phys.* **1987**, *86*, 3787.
(68) Maslen, P. E.; Faeder, J.; Parson, R. *Chem. Phys. Lett.* **1996**, *263*, 63.
(69) Stone, A. J. *The Theory of Intermolecular Forces*; Oxford: New York, 1996.
(70) Yourshaw, I.; Zhao, Y.; Neumark, D. M. *J. Chem. Phys.* **1996**, *105*, 351.
(71) Delaney, N.; Faeder, J.; Parson, R. *J. Chem. Phys.* **1999**, *111*, 651.
(72) Delaney, N.; Faeder, J.; Parson, R. *J. Chem. Phys.* **1999**, *111*, 452.
(73) Faeder, J. The X_2^- files: Modeling structure and dynamics of solvated molecular ions. Ph.D. Thesis, University of Colorado, 1998.
(74) Kohmoto, M.; Watanabe, T. *J. Phys. Soc. Jpn.* **1977**, *42*, 246.
(75) Rerat, M.; Pouchan, C. *Phys. Rev. A.* **1994**, *49*, 829.
(76) Faeder, J.; Delaney, N.; Parson, R. Manuscript in preparation.
(77) The electronic coupling matrix elements in the Case (c) representation are linear combinations of the Case (a) matrix elements, which can be thought of as arising from atomic p orbitals that have been tilted away from the internuclear axis by angles of 30, 60, and 90°.
(78) Since the spin degrees of freedom have now been included in the electronic structure, each of these six states is itself doubly degenerate by Kramers' Theorem and the dimension of the state space is actually twelve. This Kramers duplicity is rigorously preserved by all interactions within the system, so it plays no role in the interpretation of the dynamics and for the purposes of our discussion can be neglected.
(79) Strictly speaking, these are not true adiabats because they are not eigenvalues of the full 6×6 electronic Hamiltonian matrix, but only of the 2×2 blocks corresponding to pairs of diabats that cross at $\Delta\Phi = 0$. As a result these curves cross at large $\Delta\Phi$; in the true adiabats these crossings are avoided. We may regard them as belonging to an intermediate representation which exactly diagonalizes the electronic Hamiltonian only at $\Delta\Phi = 0$ but approximately diagonalizes it everywhere away from the large $\Delta\Phi$ crossings.
(80) Husain, D.; Donovan, R. J. In *Advances in Photochemistry*; Pitts, J. N., Jr., Hammond, G. S., Noyes, W. A., Jr., Eds.; Wiley-Interscience: New York, 1971; Vol. 8, pp 1−75.
(81) Delaney, N. Understanding the photodissociation dynamics of molecular cluster ions. Ph.D. Thesis, University of Colorado, 1999.
(82) Bergsma, J. P.; Berens, P. H.; Wilson, K. R.; Fredkin, D. R.; Heller, E. J. *J. Phys. Chem.* **1984**, *88*, 612.
(83) Davies, E. B. *Quantum Theory of Open Systems*; Academic: New York, 1976.
(84) Percival, I. *Quantum State Diffusion*; Cambridge: New York, 1998.